An injectable antibacterial hydrogel with bacterial-targeting properties for subcutaneous suppuration treatment

An injectable antibacterial hydrogel with bacterial-targeting properties for subcutaneous suppuration treatment

Yongchang Tian[a], Rong Zhang[a], Jiaming Cui[a],Yaowei Zhu[a], Minghui Sun[d], Ian W Hamley[c], Chunsheng Xiao[b], Li Chen [a*]

[a] Department of Chemistry, Northeast Normal University, Changchun 130024, P. R. China

[b] Key Laboratory of Polymer Ecomaterials, Changchun Institute of Applied Chemistry, Chinese Academy of Sciences, Changchun 130022, P. R. China

[c] Department of Chemistry, University of Reading, PO Box 224 Reading, RG6 6AD, UK

[d] Department of Dermatology, China-Japan Union Hospital of Jilin University, Changchun, 130033, P.R. China

[*] Corresponding author.

E-mail addresses: chenl686@nenu.edu.cn

Abstract

Purulent infections present challenges to medical procedures and burden patients with drainage procedures. An injectable antibacterial hydrogel can be directly administered to the infected tissue through a syringe, making it one of the most effective strategies for treating subcutaneous infections. In this study, we utilized an injectable hydrogel (PHP gel) with targeted bactericidal properties for surgery-free treatment of subcutaneous infections. The PHP gel was cross-linked using the Schiff base reaction between amino-functionalized polyhydromethylpyrimidine (PHP-NH_2) and oxidized dextran (o-Dex). PHP-NH_2 possesses the ability to kill bacteria through electrostatic interactions, while o-Dex enhances bacterial targeting by binding to lectins on the bacterial outer membrane ***via*** sugar units. *In vitro* experiments demonstrated that the PHP gel effectively eradicated 100 % of pathogenic bacteria within 2 hours. Moreover, when used *in vivo* for treating purulent subcutaneous infections, the injectable PHP gel exhibited remarkable efficacy by preventing infection progression and eliminating pustule tissue within 24 hours. Importantly, no significant adverse effects on blood or organ systems were observed in mice treated with PHP gel. Therefore, this polysaccharide- and polyhydropyrimidine- based hydrogel material holds immense potential as a novel antibacterial agent for managing purulent subcutaneous infections.

Key words: antibacterial, injectable hydrogel, non-surgical treatment, polyhydropyrimidine, purulent infection

1. Introduction

Microbial infections have long been implicated as the most formidable menace to public health and safety[1]. Once bacteria invade the body, they rapidly utilize nutrients in the surrounding environment to multiply and cause significant damage to local tissues[2]. Compared to other pathogenic bacteria, pyogenic bacteria have a stronger ability to proliferate and secrete extracellular polymeric matrix[3]. They can quickly colonize the invasion site and form multi-layer biofilms[4]. Once the biofilm matures and develops suppurative lesions, the bacterial flora's resistance to antibiotics dramatically increases, sometimes reaching levels of resistance nearly a thousand times higher, rendering certain antibiotics completely ineffective[5,6]. Additionally, non-open infections with tiny wound invasion are even more troublesome compared to open wound infections[7]. For instance, in daily life, purulent subcutaneous infections commonly occur due to needle puncture injuries. The purulent bacterial biofilm gradually destroys the skin tissue from within until complete necrosis and ulceration[8,9]. Apart from surgical drainage, there are no other clinical solutions available for non-open purulent bacterial infections[10]. However, surgical drainage not only causes secondary tissue damage but also requires frequent equipment replacement without anesthesia, which imposes a significant physical and psychological burden on the patient[11,12]. Therefore, it is crucial to develop more efficient treatments for non-open purulent bacterial infections.

An injectable hydrogel can be applied to the lesion through a syringe, causing almost no secondary harm to the patient compared to surgery. As a representative biomaterial, hydrogels possess highly flexible properties that make them excellent medical

substrates[13]. For instance, Ding and colleagues introduced dynamic covalent bonds into the gel to enable injectability and self-healing. This allows the gel dressing to dissolve upon demand, avoiding secondary damage caused by frequent dressing changes and significantly expediting wound healing[14]. The administration of injectable hydrogel aligns with the treatment requirements for non-open wound infections, offering the possibility of removing subcutaneous suppuration without resorting to surgery[15,16]. Additionally, pathogenic bacteria can produce mature biofilms within pustules, thereby enhancing their resistance to antibiotics. Consequently, the selection of highly effective bactericide foses another formidable challenge in the management of purulent subcutaneous infections.

Polycationic antibacterial agents primarily act on bacterial membrane structures, thereby minimizing the risk of severe bacterial resistance[17-20]. Polyhydropyrimidine (PHP), a cationic heterocyclic polymer synthesized through multi-component polymerization, has been extensively utilized in the field of antibacterial medicine [21-23]. Li's team successfully developed a hybrid hydrogel based on a cationic polypentahydropyrimidine library with remarkable modifiability and therapeutic efficacy for treating infectious diabetic foot ulcers [24]. Hence, PHP can effectively serve as the fundamental framework for constructing the antibacterial gel. Apart from their bactericidal effects, enhancing bacterial targeting is another crucial aspect to consider in designing antibacterial biomaterials[25-29]. Bacteria express numerous non-enzymatic lectins in their free phase to form biofilms[30]. These proteins can recognize polysaccharide structures present on bacterial outer membranes and bind with free bacteria, leading to the initial formation of bacterial aggregates that eventually

develop into stable biofilms on host surfaces[31-33]. Leveraging this characteristic by incorporating natural polysaccharides containing abundant sugar units into hydrogels as competitive targets for bacterial outer membrane lectins represents an ideal strategy for improving targeting capabilities.

Heren, an injectable antibacterial hydrogel with targeted bacterial action was designed and employed for the treatment of suppurative subcutaneous infections. As illustrated in **Scheme 1A**, the cross-linking network is predominantly established through both Schiff base reactions and hydrogen bonds between the aminated polyhydropyrimidine (PHP-NH_2) and the oxidized dextran (o-Dex). The dextran surface of the hydrogel enhances its capacity to capture bacteria by facilitating binding action between polysaccharide units and bacterial lectins (**Scheme 1B**). Besides, upon contact or close proximity of the negatively charged membrane of the bacterium with the PHP gel within the infectious microenvironment, it undergoes adsorption onto the gel surface through electrostatic interaction. The PHP-NH_2 further adsorbs onto the outer surface of bacteria and gradually accumulates, as depicted in **Scheme 1C**, disrupting the curvature of the bacterial membrane and dissociating a portion of its structure, ultimately leading to bacterial eradication. Furthermore, the administration of PHP gel effectively halted the progression of subcutaneous infection in murine models and ultimately achieved a complete treatment of the infection (**Scheme 1D**).

2. Results and discussion

2.1 Construction and characterization of the PHP gel.

The PHP gel was constructed by cross-linking of PHP-NH_2 and o-Dex (**Figure 1A**). Firstly, PHP was synthesized by non-catalyzed "one-pot" series polymerization [34], and the amino group was then introduced into the polymer backbone through an ammonolysis reaction to obtain PHP-NH_2 **(Scheme S1)**. The chemical structure of the polymers was determined using ^{1}H and ^{13}C NMR spectrums (**Figure S1A**). Characteristic peaks at δ = 3.64 ppm and δ = 4.21 ppm in the ^{1}H NMR spectrum confirmed the formation of hydrogenated pyrimidine repeating units, which were further indicated by the ^{13}C NMR spectrum (**Figure S1B**). After amination, changes were observed in **Figure S2** including disappearance of characteristic peak attributed to methyl ester and appearance of characteristic peak for ethylenediamine methylene. Subsequently, the chemical structures of PHP-NH_2 and o-Dex were further confirmed through FTIR spectroscopy. As shown in **Figure S3A**, the appearance of a broad peak centered around 3400 cm^{-1} in the FTIR spectra of PHP and PHP-NH_2 provides even more compelling evidence for the grafting of amino groups. For the o-Dex, after oxidation with sodium periodate (**Scheme S2**), new peaks at 1724.15 cm^{-1} correspond to aldehyde groups **(Figure S3B**), which are absent in the Dex spectrum, thus offering persuasive proof for the successful oxidation of glycosidic bonds. The oxidation degree and specific aldehyde content of o-Dex were determined using the hydroxylamine hydrochloride acid-base titration method, yielding an oxidation degree of 33 %. Finally, the PHP gel could be rapidly prepared through the simple mixing of various component solutions. The PHP gel exhibits a sustained elasticity across various formulations, remaining impervious to deformation even after being inverted for a duration of 30 seconds (**Figure S3B**). Comparison of the FTIR spectra of

freeze-dried PHP gel and raw materials provides further evidence for the formation of the gel network. As shown in **Figure S5**, the characteristic peaks attributed to PHP-NH_2 in the spectrum of PHP gel at 2992.37 cm^{-1} and 2884.21 cm^{-1} were observed, while a significant enhancement of the characteristic peaks at 1218.96 cm^{-1} and 782.32 cm^{-1} were also observed.

2.2 Rheological performance, injectability, and self-healing properties of PHP gel.

The introduction of dynamic chemical bonds gives the hydrogel both self-healing properties and injectability[35]. The PHP gel demonstrates a highly elastic state under static conditions, the modulus *G*' greater than *G*" was observed across the measured frequencyrange at low strain (**Figure 1A)**. This observation indicates that the PHP gel exhibits no flow behavior and can therefore potentially remain within the lesion tissue for an extended period. However, as the strain increases, it can be observed from **Figure 1B** that *G'* rapidly falls below *G"* when subjected to a strain of 478 %, showcasing the destruction of the gel network and its transformation from a highly elastic state into a viscous flow state. Moreover, the viscosity of the gel experiences a significant decrease with increasing shear strain (**Figure 1C**). We subsequently conducted an *in vitro* injection of PHP gel using a 1 mL medical syringe, successfully achieving precise control over gel injection and even enabling effortless writing (**Figure 1C**). Subsequently, rheological tests were conducted on the PHP gel under alternating strain conditions, as depicted in **Figure 1D**. When the strain varied from 1 % to 500 %, the gel transitioned into a viscous flow state with *G*" > *G'*. However, upon strain withdrawal, the gel network rapidly reassembled and reverted to a highly elastic state.

Notably, no significant alteration was observed in the maximum value of storage modulus after three cycles. After undergoing multiple injection cycles, the PHP gel was collected and examined using a scanning electron microscope (SEM) to investigate its microscopic morphological changes. The initially formed PHP gel, as depicted in **Figure 1E**, presents a pore wall that remained fully intact. After one injection, noticeable fractures appeared on the pore wall; however, its overall integrity was still maintained.

Interestingly, starting from the second injection cycle, the cross-linked network of the PHP gel gradually transformed from three-dimensional pores into a silk-like structure with a three-dimensional appearance. The morphology observed after the third injection showed no significant differences compared to that after the second injection. We hypothesize that this phenomenon can be attributed to destruction of the gel during the second injection cycle, leading to localized pulling forces during network remodeling and ultimately resulting in formation of a "silky flocculent" network structure. This model construction method was employed to further validate the impact of multiple cycles on the performance of PHP gel. As depicted in **Figure 1F**, the dyed PHP gel maintains capacity for seamless healing upon contact, while retaining exceptional elasticity under traction forces and ultimately achieving complete restoration according to the predetermined shape. Surprisingly, PHP gel demonstrates flexible adhesion on joints with a wide range of motion. As shown in **Figure 1G**, PHP gel maintains its initial shape even after the knuckle is bent at 90°. These findings validate the dynamic nature of PHP gel from both mechanistic and experimental

perspectives, thereby establishing a solid foundation for its prolonged residence at the infected site.

2.3 *In vitro* antibacterial properties and antibacterial mechanism of free PHP-NH_2.

The bactericidal property and antibacterial mechanism of PHP-NH_2 were tested *in vitro*. The minimal inhibitory concentration (MIC) of PHP-NH_2, as depicted in **Figure 2A**, was determined using the optical density method as about 50 μg/ ml for *S.aureus* and 100 μg/mL for *E.coli* respectively. In the weakly alkaline environment of bodily fluids, bacteria are electronegative, rendering them vulnerable to cationic antibacterial agents that disrupt their membranes. As illustrated in **Figure S6**, the bacterial zeta potential measures approximately -10.6 mV for *S.aureus* and -12.4 mV for *E.coli*. The free PHP-NH_2 demonstrates a positive charge of approximately 17.6 mV in the same environment, thereby inducing robust electrostatic attraction towards bacteria. With increasing concentration of PHP-NH_2, there is an upward trend observed in the zeta potential of bacteria. Interestingly, when the concentration reaches the MIC for both bacterial strains, their zeta potentials exhibit an approximately electroneutral state (**Figure S7**). Based on these results, it could hypothesized that the mechanism of action between PHP-NH_2 and bacteria may resemble the "carpet" sterilization model. As shown in **Figure 2B**, PHP-NH_2 initially adsorbs to the surface of bacteria through electrostatic interactions and accumulates gradually, disrupting charge balance within the bacterial cell membrane and causing disorder in its permeability. This leads to leakage of bacterial contents until a threshold level is reached where a steady-state structure cannot be maintained. To validate the inference, the depolarization

process of the bacterial cell membrane was monitored using the 3,3'-Dipropylthiadicarbocyanine Iodide (DiSC3(5)) fluorescent probe (**Figure 2C**). Polymyxin B and PBS were employed as control groups, with ε-polylysine (PLL) as a polymer cation reference model. Upon treatment with different cationic antibacterial materials, a rapid increase in microbial membrane fluorescence intensity was observed within 2 minutes, indicating the depolarization of the microbial outer membrane. Moreover, these materials were faster acting against *S.aureus*. Considering the extent of depolarization, PHP-NH_2 exhibits greater potency towards plasma membrane-rich *E.coli* compared to PLL with higher charge density. However, it shows slightly reduced efficacy against *S.aureus*. This phenomenon could be attributed to the inherent characteristics of the two microorganisms. *E.coli* possesses a significantly larger volume compared to *S.aureus*, featuring a double plasma membrane separated by a periplasmic space. Consequently, this leads to a reduction in the enrichment of macromolecules such as PHP-NH_2 on its surface. On the other hand, *S.aureus* exhibits an outer surface enriched with a peptidoglycan wall composed of high-density teichoic acid residues, which imparts it with higher electronegativity. This heightened electronegativity renders it more susceptible to cationic materials. The transmission electron microscope (TEM) images from ultra-thin section of the bacteria further substantiated the aforementioned observation. As depicted in **Figure 2D**, compared with PBS groups, both *E.coli* and *S.aureus* exhibited internal cavities partially induced by loss of bacterial cell content at the MIC concentration after 4-hour incubation with PHP-NH_2. At this stage, PHP-NH_2 disrupted the potential balance of bacterial outer membrane, leading

to depolarization behavior. Upon extending the incubation time to 8 hours, a significant leakage of bacterial content was observed, particularly pronounced in *S.aureus*. Bacteria struggled to maintain structural stability as their unsupported cell membranes contracted inwards, resulting in a "plasmolysis" state for *S.aureus* (red arrow). Finally, after 12 hours of incubation, it can be seen that PHP-NH_2 has completely disrupted the bacterial architecture. The cell membrane and cell wall of *E.coli* exhibited multiple perforations, while the remaining portion of *E.coli* displayed plasmolysis (indicated by the yellow arrow), which was consistent with observations in *S.aureus*. Meanwhile, burst-like damage was observed in the cell wall and cell membrane of *S.aureus*. An interesting phenomenon shows that only when reaches a specific concentration on the bacterial surface does PHP-NH_2 exhibit a pronounced destructive effect on the bacteria.

To further validate the membrane-breaking antibacterial mechanism, the modified concentration-dependent SYTO-9/PI double-staining experiments were performed[36]. As depicted in **Figures 3A and 3B**, before reaching the MIC concentration, both *E.coli* and *S.aureus* exhibited green fluorescence upon staining with SYTO-9, while minimal red fluorescence was observed using the PI probe. Concurrently, the formation of bacterial was evident in the incubated bacterial solution. Upon reaching the MIC concentration, a conspicuous presence of red fluorescence was detected, accompanied by an absence of colonies after incubation, thereby indicating concordance between the MIC of PHP-NH_2 and the minimum bactericidal concentration (MBC). Interestingly, a positive correlation between the concentration of PLL and the degree of sterilizing ratio was observed in the repeated

experiment. As depicted in **Figure S8**, at 0.6 times the MIC concentration, certain bacterial membranes were destroyed (red fluorescence), and a significant reduction in colony count was evident after an overnight culturing. For PHP-NH_2, only a bactericidal ratio of approximately 9 % (**Figure 3C**) was found at 0.8 times MIC concentration, while PLL achieved a level close to 47 % (**Figure 3D**) in the same conditions. From the perspective of merged bacterial fluorescence ratio (**Figure 3E**), about 76% of bacteria were affected by PLL treatment, indicating that nearly 29% of the surviving bacteria experienced membrane damage and could not impede the entry of PI probe, resulting in false positives. The findings suggest that PHP-NH_2 exhibits a concentration-dependent bactericidal mode with "mutant" sterilization behavior, whereas PLL demonstrates a concentration-dependent bactericidal mode with "cumulative" sterilization behavior. This implies that the drug effect of PHP-NH_2 is comparatively milder and will possess bioaffinity at concentrations below MIC, thus enhancing its potential as an antibacterial agent.

2.4 *In vitro* antibacterial properties and antibacterial mechanism of PHP gel.

A hydrogel material with a cross-linked structure can maintain a highly elastic form and stay in pustules, which is more suitable than intravenous administration[21]. After gelation of the PHP gel, a high density of cations surface was formed by PHP-NH_2 and attracted electronegative microorganisms through electrostatic interaction (**Figure 4A**). The bactericidal performance of PHP gel was evaluated by comparing it with a clinically bactericidal chitosan quaternary ammonium gel (QCS gel) as the positive control. A significant reduction of colonies was observed after incubation of the bacterial suspension

with both gels for varying durations. Within 120 minutes, both gels exhibited cumulative bactericidal effects on *E.coli* (**Figure 4B**) and *S.aureus* (**Figure 4C**); however, PHP gel demonstrated superior efficacy compared to QCS gel (**Figure 4D and E**). Significantly, the bactericidal efficacy of PHP gel demonstrated a notable enhancement during the co-incubation period of 40-60 minutes, resulting in a remarkable 40% reduction in bacterial survival rate. This phenomenon could be attributed to the cleavage of Schiff base bonds triggered by the acidic metabolites from bacteria during this time frame, resulting in release of PHP-NH_2, thus accelerating bacterial eradication. The action mode and efficiency of PHP gel were further investigated using the live-death staining method. As depicted in **Figure 4F and 4G**, both *E.coli* and *S.aureus* exhibited intense red fluorescence after a 20-minute exposure to PHP gel, with a merged ratio close to 90%. However, the bacterial survival rate remained around 75% from the LB medium culture result. This false positive phenomenon suggests that most bacteria have already undergone non-lethal reversible membrane damage. Furthermore, SEM images revealed noticeable surface shrinkage of the bacteria after 20 min, particularly more severe in *E.coli* compared to *S.aureus*. This disparity may be attributed to the larger rod-shaped volume of *E.coli* compared to the spherical shape of *S.aureus*, making it more susceptible upon contact with the hydrogels. The PHP gel effectively eradicated all bacteria upon contact after 120 minutes, with no significant difference observed in the action time between *E.coli* and *S.aureus*. These findings demonstrate that the PHP gel can efficiently eliminate microorganisms through its dynamic cationic surface following gelation. Furthermore, when the contact time exceeds 40 minutes,

it can release PHP-NH_2 by dissociating the local gel structure, thereby further enhancing its bactericidal efficacy. This "stimulation-enhanced" bactericidal strategy endows the PHP gel with both the capability to combat bacterial infections and long-term retention ability in stubborn pustules.

In addition to electrostatic interactions, the strong affinity of PHP gel towards bacteria is also due to lectin-dextran interaction. To investigate and quantify the correlation between these two bacterial targeting mechanisms, we utilized polymer fluorescence labeling and gel surface adsorption assays. As shown in **Figure S9**, the Rhodamine B-labeled PHP polymer is strongly bound to bacteria, resulting in a strong red fluorescence for both bacteria. Similarly, the FITC-labeled Dex exhibited strong green fluorescence when incubated with bacteria alone. Interestingly, PHP-RhB caused distortions in the shape of *E.coli*, resulting in obvious depressions as indicated by the white arrows. However, no depression of the bacteria was observed in the Dex-FITC image. This may be because the grafting of the hydrophobic dye Rhodamine B accelerated the movement of PHP molecules into the bacterial phospholipid membrane, making the effect more obvious. However, the electrically neutral Dex-FITC cannot be attracted by the electronegative phospholipids, and thus accumulates on the periphery of the bacteria and is isolated by the cell wall, so the depression of the lipid inner membrane cannot be observed.

Additionally, as depicted in **Figure S10**, a polysaccharide-free gel PHP/P(DMA-VA) was synthesized by employing an acrylate polyaldehyde-based polymer and PHP-NH_2. As the other control group, the o-Dex/ADH gel cross-linked with adipic acid dihydrazide (ADH) was

chosen to assess the impact of these two mechanisms on bacterial adsorption capacity on the gel surface. Surprisingly, as shown in **Figure S11**, PHP gel exhibited the highest bacterial capture ability for both bacteria. The number of *E.coli* adsorbed on the surface within one hour was approximately 45.6×10^5 CFU. Without polysaccharide, PHP/P(DMA-VA) gel only captured 21.4×10^5 CFU, which is half of the capacity of the PHP gel capacity. However, it still surpassed the adsorption capacity of o-Dex/ADH gel (a polysaccharide gel without polypyrimidine structure), which was 15.96×10^5 CFU. These results demonstrate that introducing a polysaccharide structure does enhance the gel's bacterial capturing ability, but its main targeting effect remains electrostatic adsorption of cationic polymers. The two gels with polypyrimidine backbone had much higher bacterial adsorption capacity (PHP gel~153.68×10^5 CFU, PHP/P(DMA-VA) gel~110.04×10^5 CFU) compared to the targeting ability of o-Dex/ADH gel~45.12×10^5 CFU, while showing similar effects on *S. aureus.* This difference in bacterial capture ability is attributed to variations in bacterial structure, as the cell wall of *S. aureus* contains multiple layers of electronegative teichoic acid and is smaller than *E.coli*, making it more susceptible to electrostatic attraction. *E.coli*, with its double-layered cell membrane and larger size, has an elongated structure that increases the surface contact between membrane and the gel. Therefore, surface lectins are more susceptible to the influence of polysaccharides. These results indicate that although electrostatic interactions resulting from polypyrimidine structures play a major role in bacterial adhesion ability, the introduction of polysaccharide molecules significantly

enhances the ability of the gel to trap bacteria, especially Gram-negative bacteria, thereby enhancing its effectiveness.

2.5 *In vitro* biosafety test of PHP gel.

In principle, the PHP gel has a distinct sterilization property compared to that of free antibacterial agents, since the gel reduces the spread of PHP-NH_2 to normal tissues while retaining its high-efficiency bactericidal properties and ensuring optimal biological safety. To validate this hypothesis, we utilized L929 cells as a model to comprehensively assess the cytocompatibility of PHP gel from three perspectives: concentration-dependent cell viability, time-dependent cell proliferation ability, and cell migration capacity. As shown in **Figure 5A**, at a concentration of 1000 μg/mL, PHP gel demonstrated comparable cytocompatibility to the commercial Tegaderm™ gel with a cell survival rate exceeding 90%, meeting the minimum requirements for *in vivo* application. Subsequently, the concentration of 1000 μg/mL was selected to evaluate subsequent cell safety indicators. As depicted in **Figures 5B and 5C**, in the "scratch healing" experiment, at 24 hours, all three experimental groups exhibited a reduction in cell scratches and similar degrees of healing. However, at 48 hours, Tegaderm™ showed a slightly higher scratch healing rate than PHP gel and the blank group; Fortunately, the healing rate of PHP gel remained equivalent to that of the control group, indicating that although it did not possess any cell movement accelerating properties, it also did not impair cellular migration function. Except for mobility, the cell division performance was further investigated under the same gel concentration. The PHP gel was pre-placed in the transwell chamber and ensured complete submersion in the cell plate well. As depicted

in **Figure 5D**, there was a significant increase in cell density after 24 hours, and the entire culture plate well was essentially filled after 48 hours. Following Hoechst staining, it was observed that the bacterial nuclei exhibited intact shape with clear boundaries and no apparent signs of damage indicators. Cell proliferation performance, assessed by CCK-8 method, showed slightly lower results for both PHP gel and Tegaderm™ compared to blank control (**Figure 5E**), but without any significant differences between groups. These findings demonstrate that PHP gel achieves equivalent biological safety to Tegaderm™ moist wound care gel at a cellular level while providing an effective means to establish a safe moist healing environment for wounds. The toxicity of PHP gel to red blood cells was further investigated by acute hemolysis experiments. As shown in **Figure 5F**, the acute hemolysis rate of PHP gel at a concentration of 1000 μg/mL was found to be below 10%, not significantly different compared to the blank control. The above results prove that PHP gel has reached the level of commercial gel dressings in terms of *in vitro* cytotoxicity and hematocompatibility, laying a solid foundation for its next *in vivo* infection experiment.

2.6 *In vivo* evaluation of PHP gel against purulent subcutaneous infection.

The internal environment of the body is more complex than the simulated environment *in vitro*[37]. There are numerous cases of antibacterial materials where the impressive effects observed *in vitro* are accompanied by a significant reduction or even loss of therapeutic efficacy *in vivo*. Therefore, the ultimate criterion for evaluating material feasibility lies in its therapeutic effectiveness. The therapeutic efficacy of PHP gel *in vivo* was investigated via the subcutaneous infection model, and comprehensive comparison groups were conducted

with clinical products including antibiotics amoxicillin and Tegaderm™. As illustrated in **Figure 6A**, prior to the initiation of the experiment, all infected groups were subcutaneously pre-injected with strains one day in advance, and formal treatment was commenced after 12 hours of initial pustule formation. Skin sections of all experimental mice were meticulously documented, while tissue fluid puncture samples were collected and cultured at various time points for precise quantification of colony growth. The therapeutic efficacy was evaluated based on scores reflecting skin health status and quantification of colonies present in puncture fluid. As shown in **Figure 6B**, on the initial day of administration, mice in all experimental groups exhibited a smooth skin surface with soft and plump tissue, accompanied by slight swelling at the administration site. However, after 24 hours, evident rejection reactions were observed in both the infection group “SA” (*S.aureus*) and the commercial gel treatment group “Tegaderm™ + SA”. A distinct milky white area could be observed at the lesion site, indicating the disruption of the microenvironment. The extravasation of interstitial fluid leads to the development of localized edema and a reduction in hematocyte equivalents, resulte ultimately in a milky white appearance. Moreover, the mice injected with a high-concentration PHP-NH_2 solution exhibited evident scabs throughout their entire skin tissue, whereas the skin condition of the PHP gel group remained within acceptable health parameters. This observation demonstrates that elevated concentrations (2 mg/ mL) of PHP-NH_2 could indeed induce adverse stimulation in the body; however, the strategy of o-Dex gelation effectively addresses the toxicity issue associated with PHP-NH_2. On the 3rd day, evident deterioration occurred in most of the infection groups

(**Figure 6C**), with the Tegaderm™+SA, SA, and Amoxicillin+SA groups presenting purulent discharge on their skin surfaces, marking destruction of the overlying skin tissue by the infection. The area of skin necrosis in the presence of Amoxicillin+SA group was smaller than that in the SA group; however, local ulceration and pus were still observed. Fortunately, animals in the PHP gel+SA groups displayed a smooth and healthy skin surface, suggesting the control of the infection. PHP gel effectively prevented superficial erosion caused by *S.aureus* without adverse effects on normal tissues as evidenced by intact health indicators in both PHP gel-treated and blank control groups. By day five of experimentation, the PHP gel+SA group still exhibited similar skin conditions to those in the blank control group. These results demonstrate that PHP gel is more effective than amoxicillin for treating established pustules while avoiding visible adverse stimulation to normal tissues. To further assess the condition of superficial skin, infection status was quantified by enumerating the bacterial colonies in locally punctured fluid. As shown in **Figures 6D and 6E**, all infected groups exhibited noticeable colonies at the beginning of the experiment but obvious decreases of colonies were observed after one day in both the Amoxicillin+SA group and PHP gel+SA group. By the third day, no colonies were observed in puncture fluid from the PHP gel group; however, bacteria counts began to increase compared to day one in the Amoxicillin+SA group. This evidence suggests that amoxicillin could not eliminate the formed pustules effectively. Furthermore, during the final tissue fluid extraction, a decrease in colony numbers was noted for Tegaderm™+SA and SA infection groups due to necrosis of lesioned skin that could no longer sustain colony growth. The *in vivo* anti-infection experiments have

substantiated the efficacy of PHP gel in managing subcutaneous infection deterioration and mitigating bacterial-induced skin damage. Notably, a single injection of PHP gel exhibits superior local infection clearance compared to amoxicillin.

2.7 Blood parameters, pathology and immunohistochemical analysis.

Although the effectiveness of PHP gel has been validated based on macroscopic skin health indicators, further confirmation of its impact on deeper skin conditions was still required. To address this inquiry, a post-experimental pathological analysis of the animal skin samples was conducted. As illustrated in **Figure 7A**, the histological examination of HE-stained sections from the PHP gel+SA group, Tegaderm™ group, and PHP gel group revealed well-defined skin layers with distinct accessory cell organelles. Moreover, conspicuous subcutaneous fat accumulation indicated a favorable skin condition. In contrast, evident skin necrosis was observed in the Tegaderm™+SA group, Amoxicillin+SA group, SA group, and PHP solution group. Notably, after the administration of amoxicillin, infiltration of inflammatory cells was observed surrounding the dermal tissue, forming a distinctive bubble morphology. This observation indicates that the infection remains controlled with reduced necrotic area compared to other infected groups. Complete suppuration was observed from the SA group, the large cavity made it impossible for the skin to maintain local morphology. Tegaderm™ +SA group exhibited increased dermal thickness compared to the other groups. Although it effectively prevented the dissemination of bacteria to adjacent tissues, its lack of bactericidal properties hindered its ability to halt the progression of infection. Consequently, this led to an accumulation of inflammatory cells and ultimately resulted in tissue thickening.

The statistical analysis results of pathological indicators provide a more visually comprehensive representation of the treatment effect. As depicted in **Figure 7B**, the SA group exhibits the most significant abnormalities among all groups. Tegaderm™ only demonstrates a marginal deceleration in necrosis progression compared to the SA group. Although antibiotics exhibit certain efficacy, they fail to prevent subsequent infection development. Additionally, the Masson staining results demonstrated that the PHP gel+SA group, PHP gel group, and Tegaderm™ group exhibited collagen density and coverage comparable to that of healthy skin. Only the Amoxicillin group showed some residual collagen, while minimal collagen was observed in other infection groups. As shown in **Figure 7C**, statistical analysis revealed a slightly higher level of collagen in the Tegaderm™ group compared to the PHP gel group under non-infected conditions; however, no significant difference was found between these two groups.

Cytokines play a pivotal role in orchestrating diverse physiological processes within the body. To gain deeper insights into the body's response to PHP gel, such as inflammation, we employed red fluorescent labeling of representative cells and factors, enabling their comparison with DAPI-labeled cellular nucleic acids. The platelet endothelial cell adhesion molecule-1 (CD31) is widely expressed on the surface of platelets, neutrophils, and other cells, playing a crucial role in the clearance of senescent cells. As depicted in **Figure 7D**, there was a significant upregulation of CD31 molecules observed in the skin tissue from the uncontrolled infection group. In contrast, the expression level of CD31 in animal tissues treated with PHP gel remained within the normal range, consistent with that observed in

healthy mouse skin. The human IL-1 beta protein (IL-1β) and interleukin 10 (IL-10) play crucial roles in the regulation, promotion, and antagonism of inflammation. They serve as representative signaling molecules that orchestrate the body's response to acute injury and initiate the subsequent healing process. The expression of IL-1β displayed aberrant patterns, as shown in **Figure 8A**, with the PHP-NH_2 solution exhibiting the highest level of IL-1β expression. Fortunately, the IL-1β expression within the PHP gel group remained within normal range. This observation signifies that a high concentration of free PHP-NH_2 strongly stimulates the body, thereby further validating the necessity of our gelation strategy. Regarding the anti-inflammatory factor IL-10, its expression levels generally correlated with infection severity. Nevertheless, in the SA infection group, IL-10 levels were notably low or even below normal standards. This could potentially be attributed to necrotic skin tissue caused by infection impeding proper inflammation regulation. Additionally, based on the outcomes of statistical analysis, all indicators about small animal skin in the out-of-control purulent infection group exhibited irregularly heightened expression levels without attaining statistical significance, thereby further elucidating the gravity of the infection's deleterious impact on the body. Furthermore, the safety of PHP gel was confirmed through blood tests conducted on experimental animals. As shown in **Figure 8C**, no abnormalities were observed in various blood parameters such as neutrophils (NEU) and white blood cell (WBC) following clearance of infection by PHP gel in mice. Additionally, examination of vital organs (**Figure S12**) revealed normal functioning of the heart, liver, spleen, lungs, and kidneys after treatment with PHP gel without any evident pathological changes. In summary, purulent

bacteria could disrupt the skin tissue structure by decomposing collagen, destroying capillaries, and disrupting the body's inflammatory signal balance. This ultimately leads to complete local skin necrosis. However, PHP gel effectively blocks this process eliminating pustules, and maintains functions of skin as well while causing no apparent toxicity to organs.

3. Conclusions

In summary, an injectable hydrogel based on polyhydropyrimidine polymer and oxidized dextran was developed and utilized for the treatment of purulent subcutaneous infection. The dextran-cross-linked gel exhibits good biocompatibility and enhances bacterial targeting by binding to highly expressed lectins on bacterial surfaces. The PHP gel demonstrated exceptional injectability, self-healing capabilities, and adaptiveness while effectively eradicating bacteria within 2 hours. A single treatment with PHP gel proved more efficacious in curing purulent infection than amoxicillin antibiotics. Furthermore, following treatment with PHP gel, mouse skin maintained its original physiological functions without exhibiting any abnormal indicators in blood or organs during experimental testing. This case advances the research progress of antibacterial biopolymers and provides a reference for the design of enhanced targeting of antibacterial biomaterials.

Figures and Schemes

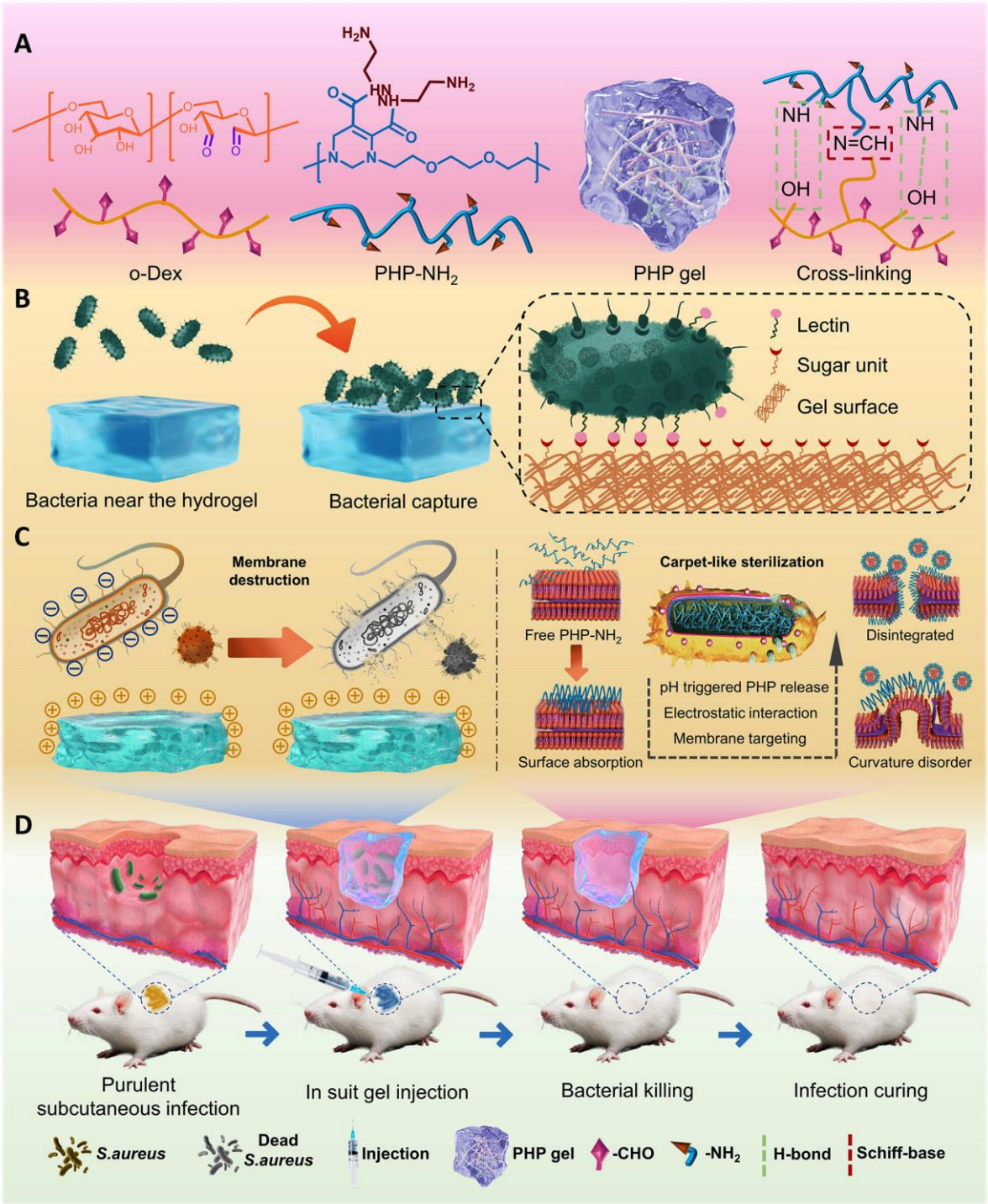

Scheme 1. Schematic illustration of the preparation and application of PHP gel. (A) PHP gel was cross-linked via both Schiff base reaction and hydrogen bonds between o-Dex and PHP-NH_2. (B) The dextran-based hydrogel surface promotes bacterial aggregation in infected tissues by facilitating the interaction between dextran and bacterial lectins. (C) PHP gel traps bacteria and destroys their outer membrane structure through electrostatic adsorption by the dynamic cationic surface, ultimately killing bacteria (D) PHP gel was used as a medicinal injection for the treatment of subcutaneous suppurative infection.

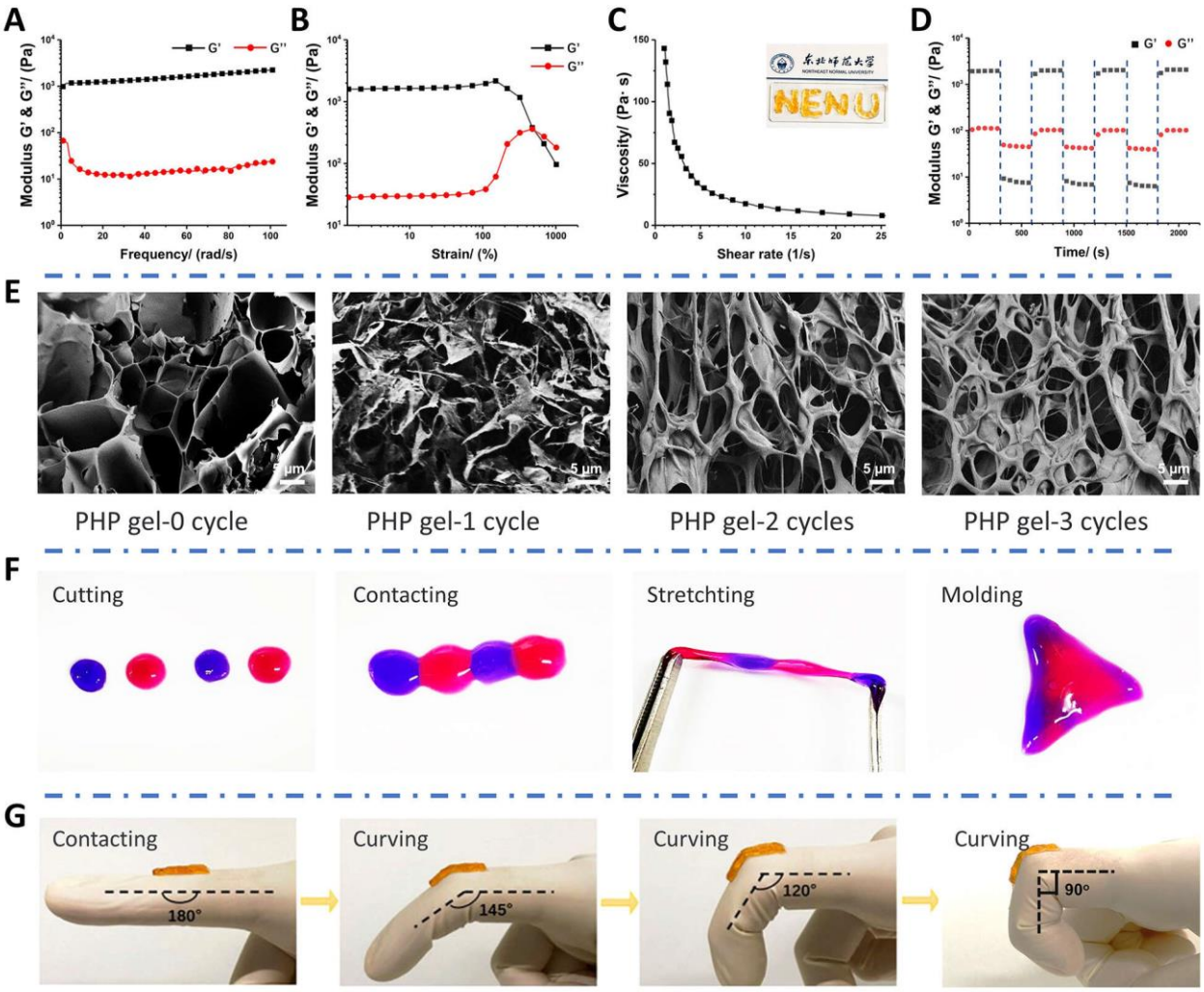

Figure 1. Characterization of the physical properties and deformation behavior of PHP gel. (A) Rheological performance test of PHP gel as a function of frequency. (B) Rheological properties of the PHP gel exhibiting strain-dependent behavior at low frequencies. (C) Viscosity behavior of PHP gels in response to shear strain and imaging of text obtained through *in vitro* injection. (D) Rheological property analysis of PHP gels under varying strains within a fixed time interval. (E) SEM images capturing microscopic morphology changes in PHP gel after different cycles of injection. (F) Evaluation demonstrating the "contact-healing" behavior of stained PHP gel, where independent clumps form strips with specific tensile strength upon contact, enabling further shaping into pre-coded forms. (G) Photograph showcasing evaluation results for flexural fit performance assessment on wrinkled articular surface.

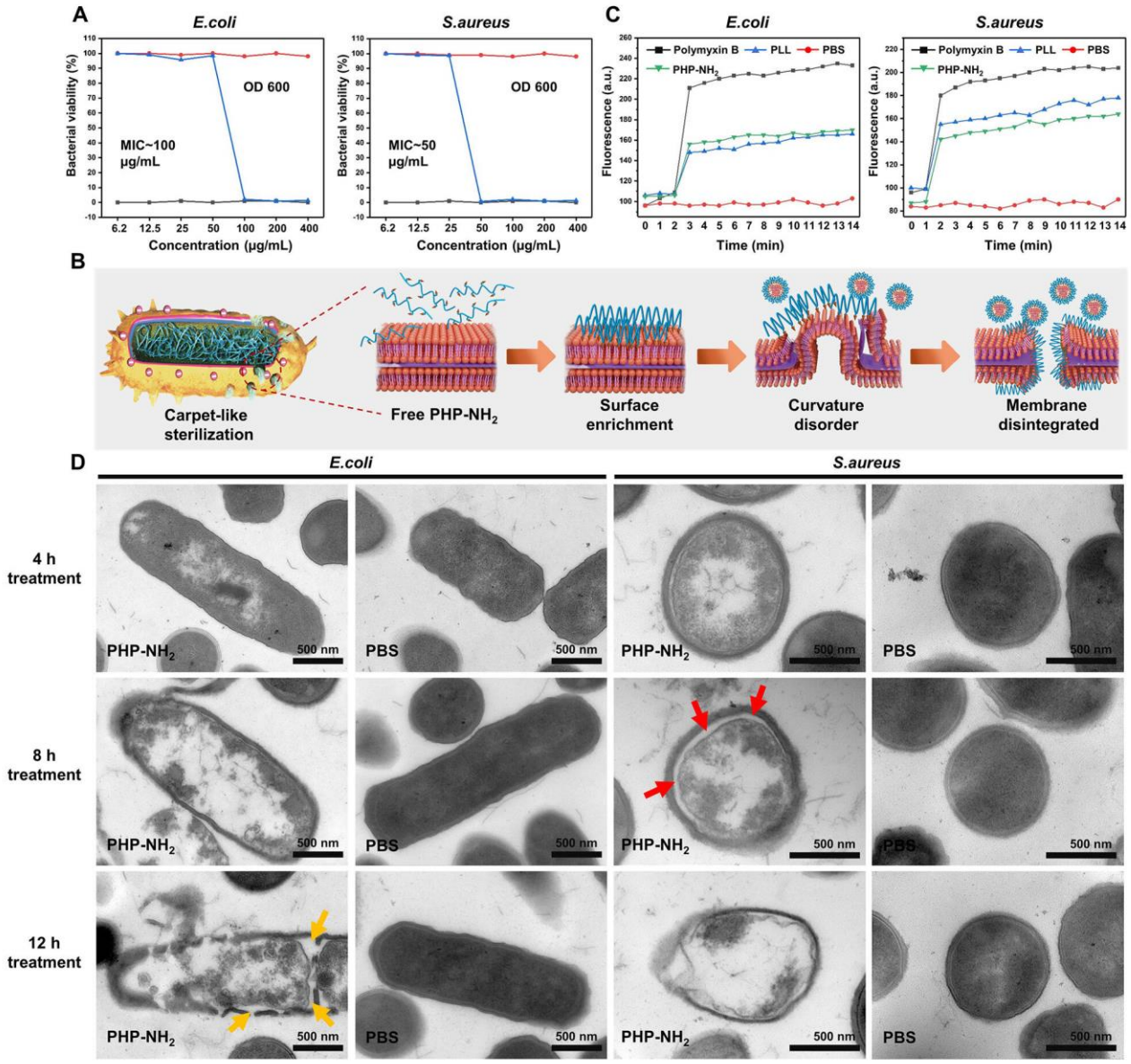

Figure 2. Antibacterial performance of PHP-NH_2 against *E.coli* and *S.aureus*. (A) MIC values of PHP-NH_2 was determined through the OD-600 optical density method. (B) Illustration of the bactericidal mechanism for PHP-NH_2. (C) Fluorescence intensity of *E.coli* and *S.aureus*, as measured by the membrane potential fluorescent probe DiSC3, after co-incubation with PHP-NH_2 solution (MIC) for varying durations. (D) TEM ultrathin section images of *E.coli* and *S.aureus* after treatment with PHP-NH_2 solution under MIC concentration and PBS for different durations.

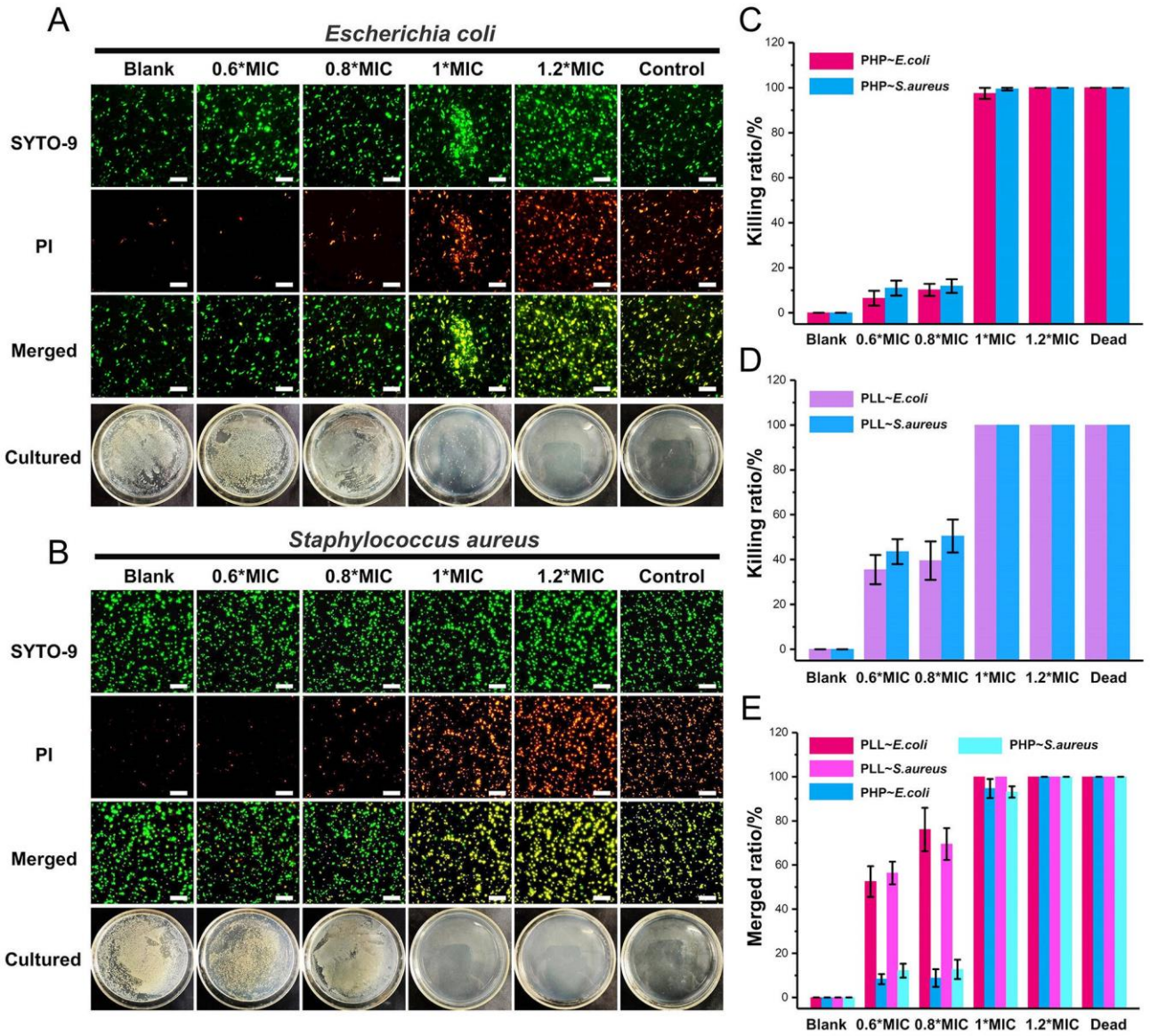

Figure 3. SYTO-9/PI bacterial live-dead double staining test results of PHP-NH_2 against *E.coli* and *S.aureus* at different MICs (Scale bar = 20 μm). Optical images collected from fluorescence microscope after incubation with PHP-NH_2 (named as PHP In the Figures) for (A) *E.coli* and (B) *S.aureus.* (C) Killing ratios for a series of concentrations of PHP-NH_2 against the two bacteria (D) Killing ratios for a series of concentrations of PLL against the two bacteria. (E) Statistical analysis of merged rate of two bacteria after incubation with PHP-NH_2 and PLL at different concentrations from fluorescence images.

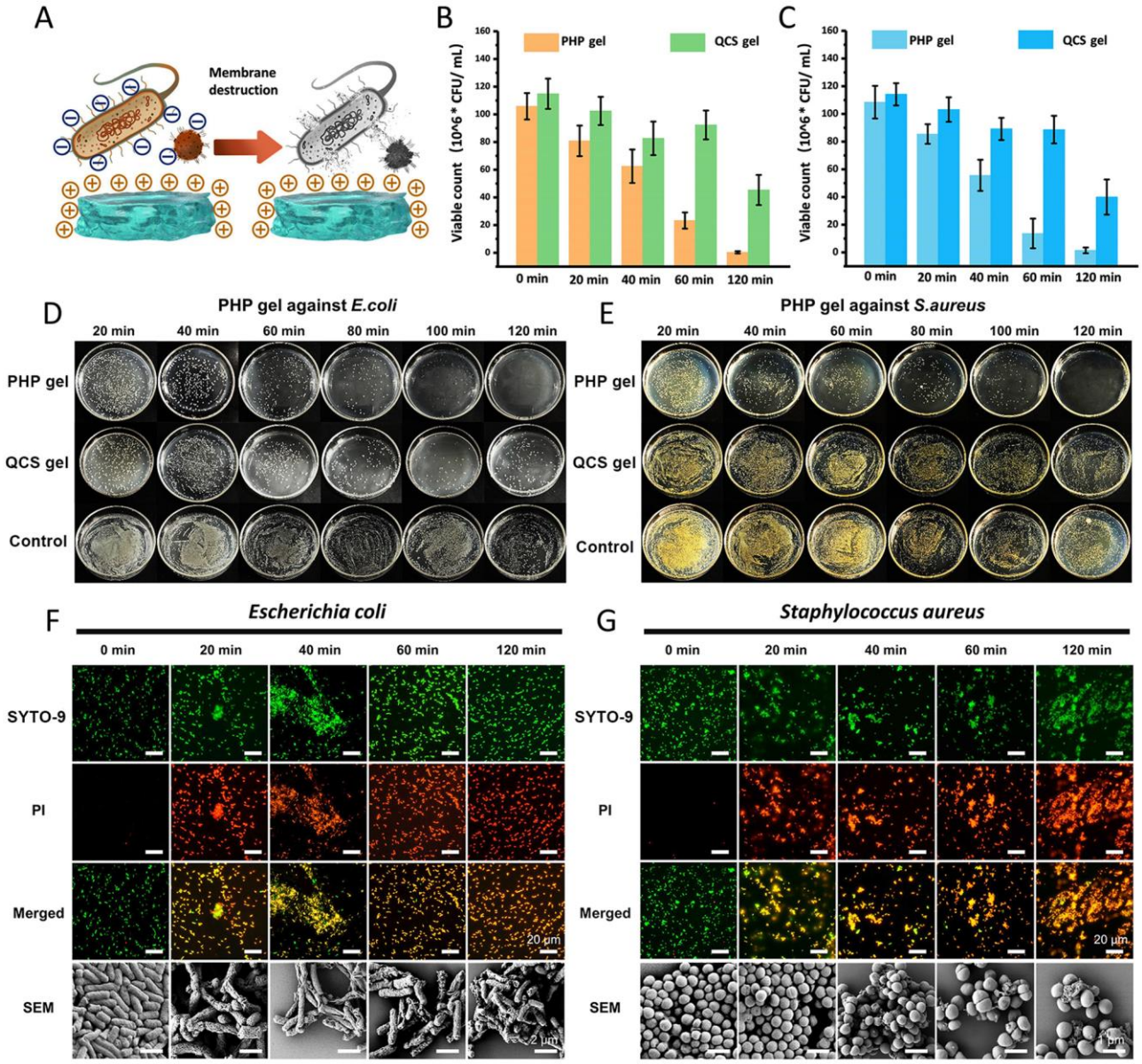

Figure 4. *In vitro* contact bactericidal performance and antibacterial mechanism of PHP gel against *E.coli* and *S.aureus*. (A) The illustration depicts the mechanism of interaction between the cationic surface of PHP gel and bacteria. Mathematical statistics of overnight incubation colonies of (B) *E.coli* and (C) *S.aureus* after treatment with PHP gel and commercial QCS gel for varying durations. Images for the colony growth of (D) *E.coli* and (E) *S.aureus* after overnight incubation on LB medium following treatment with PHP gel and. SYTO-9/PI bacterial live-dead double staining test results and SEM pictures of (F) *E.coli* and (G) *S.aureus* after being treated with PHP gel (scale bar = 20 μm).

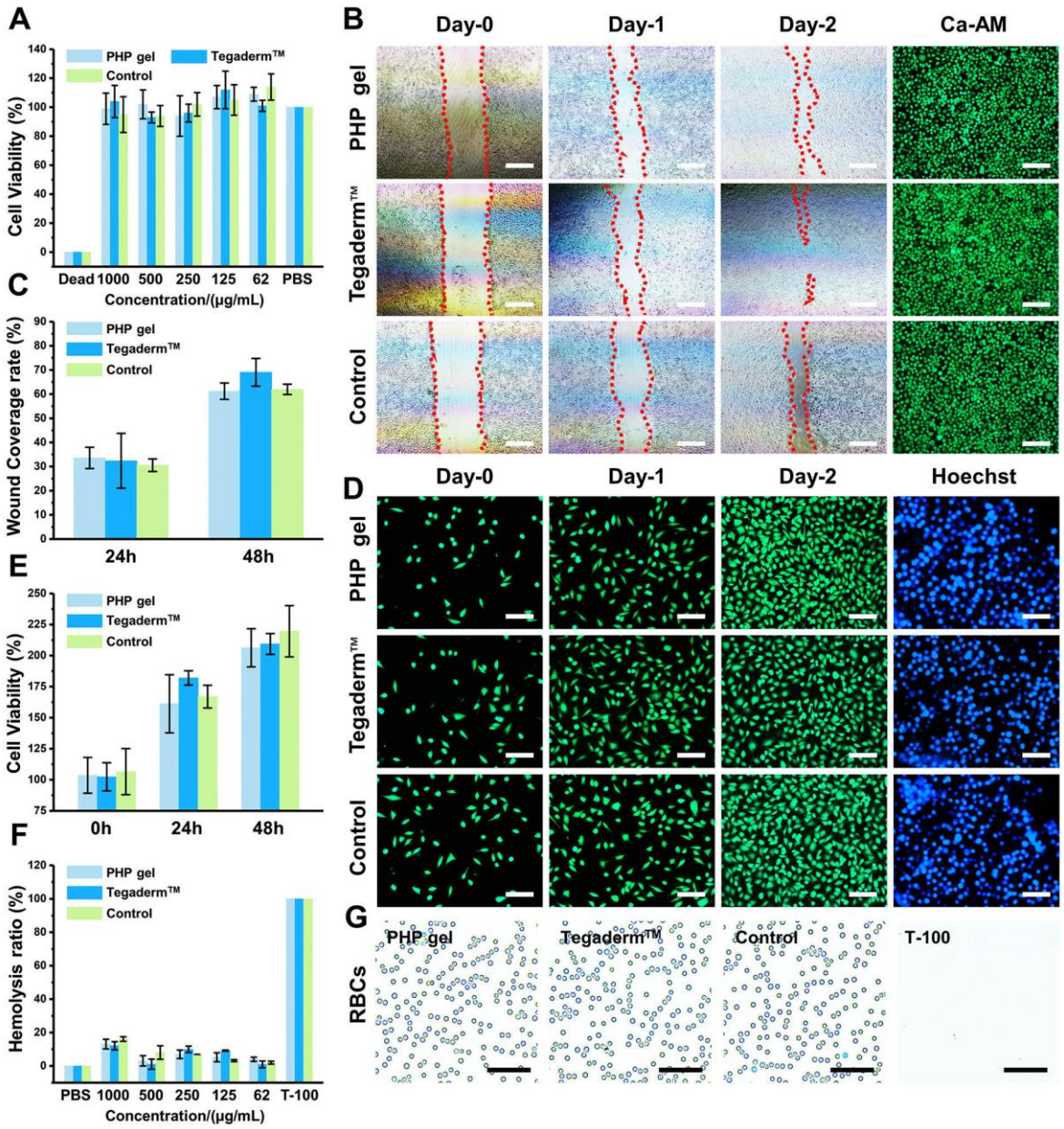

Figure 5. Biosafety assessment utilizing L929 cells and de-fiberized sheep whole blood as experimental models for PHP gel, with Tegaderm™ and PBS as the control. (A) Cell viability results of two gels at different concentrations. (B) Photographs depict the process of scratch healing of L929 cells at different time points treated with PHP gel, Tegaderm™ and Control during the "plate scratch wound healing" experiment, as well as images captured by a fluorescence microscope showing live cell probe Ca-AM staining after the conclusion of the experiment (Scale bar = 200 μm). (C) Statistical analysis of the effects of PHP gels and experimental groups on cell migration by determining the rate of scratch healing. (D) Ca-AM probe calibrated fluorescent photos of living cells treated with PHP gel and other experimental groups, and Hoechst calibrated nuclei fluorescent images after the experiment (Scale bar = 100 μm). (E) Statistical analysis of the effects of PHP gels and experimental groups on cell proliferation by quantifying the number of viable cells. (F) Optical images of fresh red blood cells incubated with PHP gel and other experimental gels. (G) Results of acute hemolytic activity of PHP gel and other experimental groups (Scale bar = 100 μm).

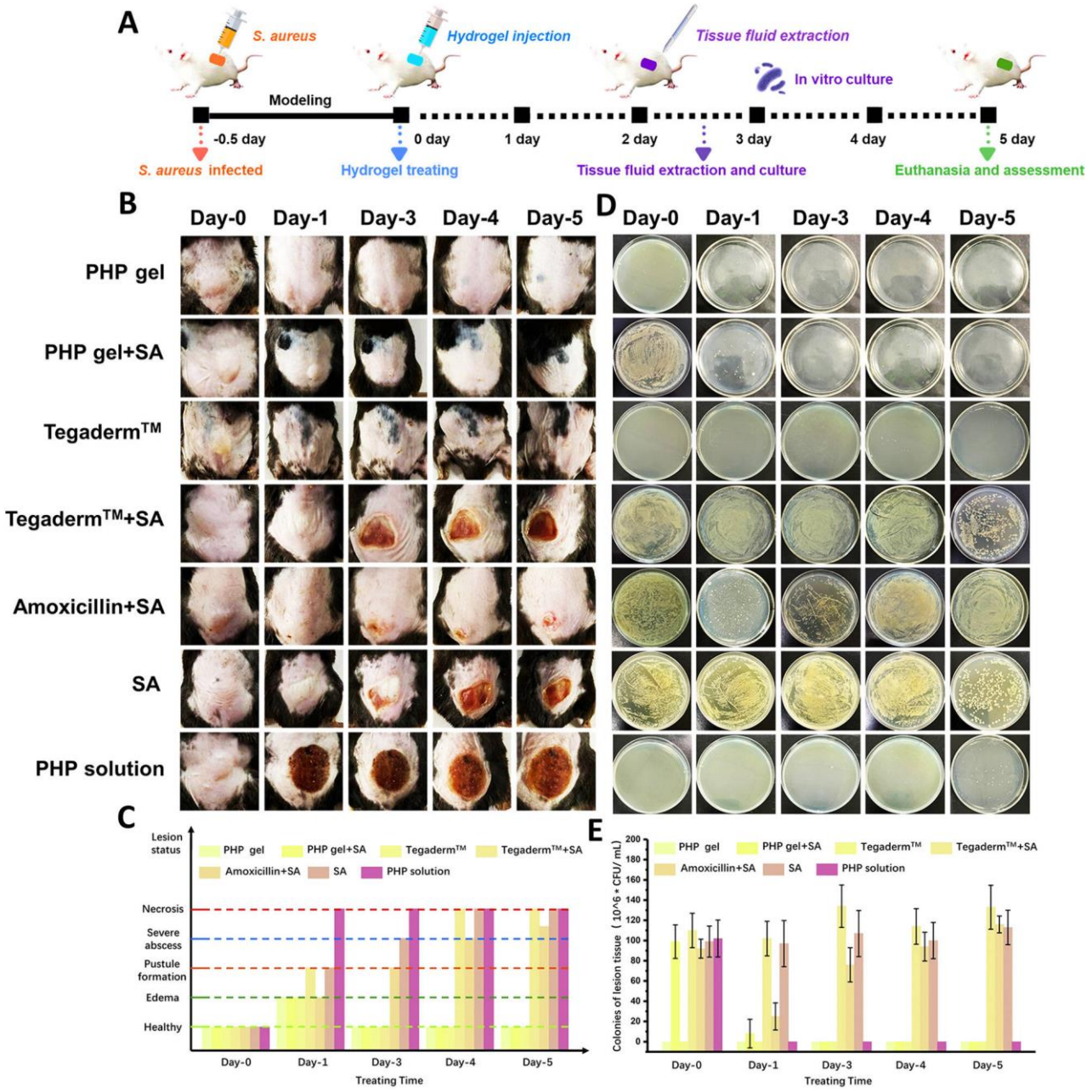

Figure 6. *In vivo* bactericidal performance of PHP gel: (A) Schematic diagram of establishment of subcutaneous infection model and gel treatment process (B) Representative images of the skins treated by PHP gel, PHP gel+SA, Tegaderm™, Tegaderm™+SA, Amoxicillin+SA, SA, and PHP-NH_2 solution (n = 6) respectively at different time points. (C) An index score of skin damage degree of animals in different experimental groups. (D) Images and (E) statistical analysis of the growth status of the animal skin puncture fluid colony in the experimental group after undergoing *in vitro* culture.

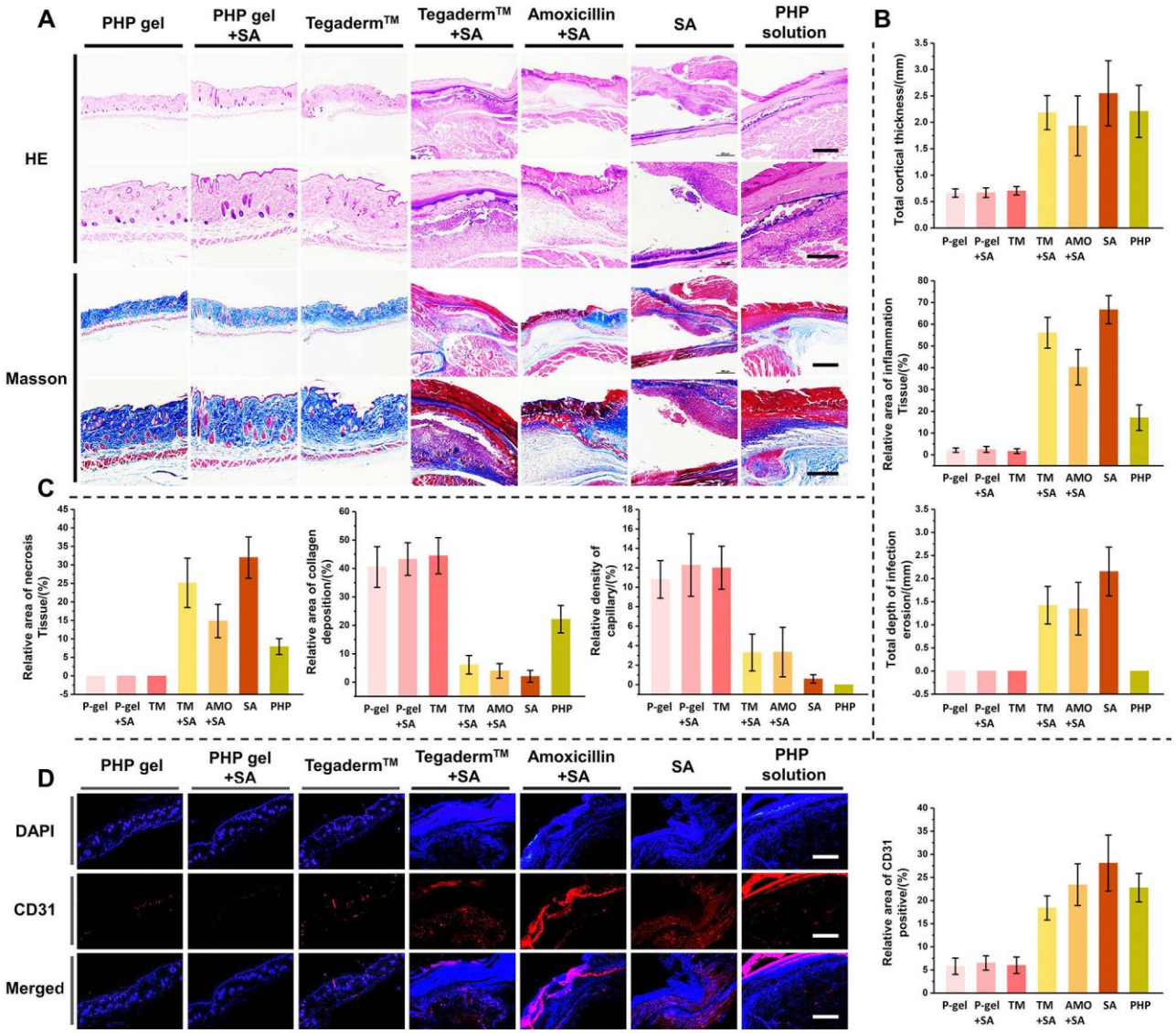

Figure 7. Histopathological and immunohistochemical analysis of animal anti-infection *in vivo*. (A) Images of the tissues after Hematoxylin-Eosin staining and Masson staining (Scale bar = 100 μm). Statistical analysis of the different indicators of (B) total cortical thickness, relative area of inflammation tissue, total depth of infection erosions; (C) relative area of necrosis tissue, relative area of collagen deposition, and relative density of capillary, respectively. (D) Immunofluorescence staining histochemical analysis of CD31 (red) signal molecule, with nuclei stained by DAPI (blue) (Scale bar = 100 μm).

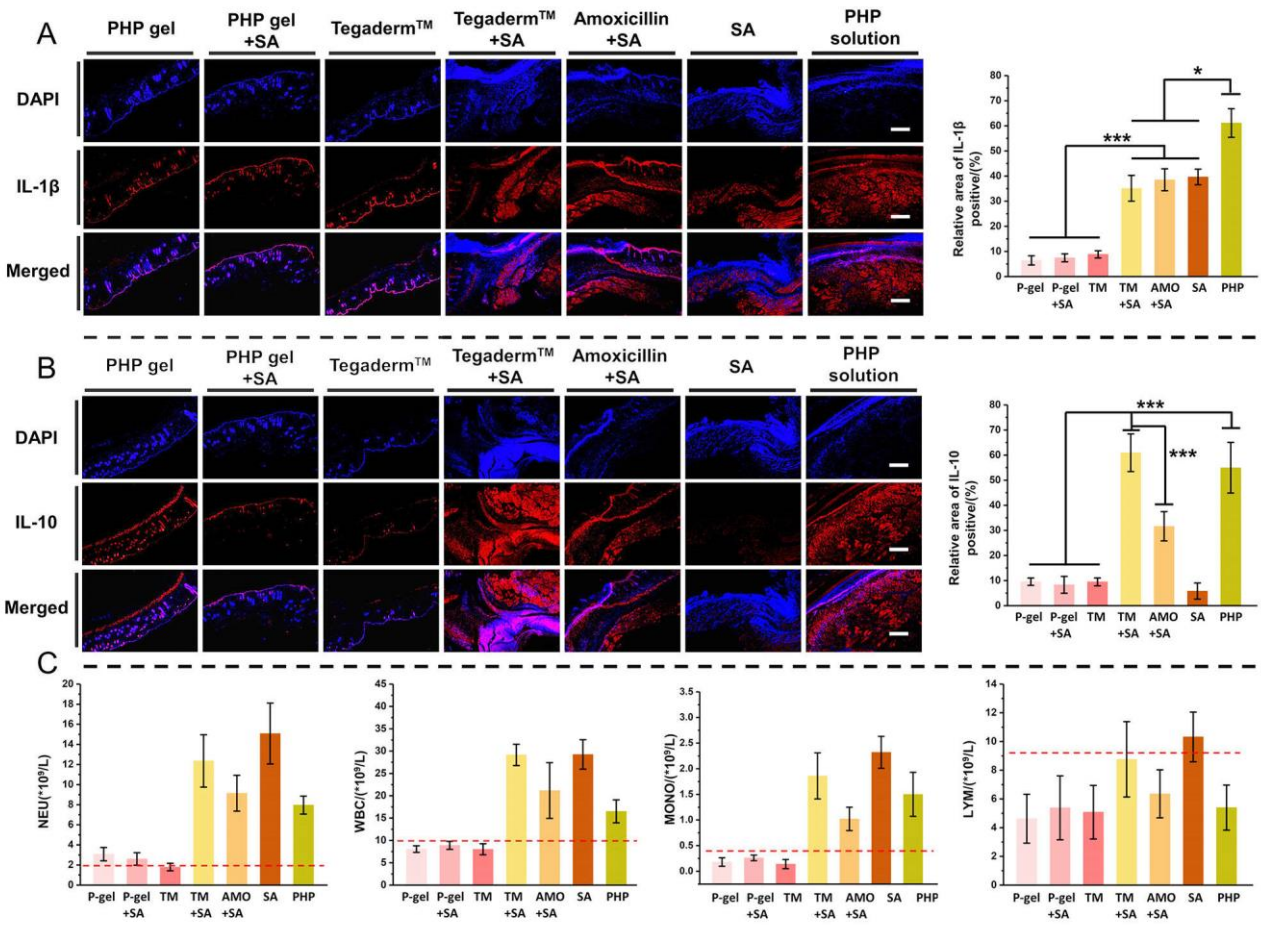

Figure 8. Immunofluorescence staining images and statistical analysis for cytokines of (A) IL-1β and (B) IL-10, respectively. (C) Routine blood test of the experimental groups (Scale bar = 100 μm).

Acknowledgments

This research was financially supported by the National Natural Science Foundation of China (51973025 and 52222307), the Jilin Science and Technology Bureau (20220204107YY and 20230204086YY), Changchun Science and Technology Bureau (21ZGY06), Jilin Province Development and Reform Commission (2023C028-4).

Declaration of Competing Interest

The authors declare that they have no known competing financial interests or personal relationshipsthat could have appeared to influence the work reported in this paper.

References

[1] D. Li, X. Dong, X. Liu, H. Lin, D. Yang, X. Shi, C. Chen, F. Tao, L. Jiang, H. Deng, Cellulose nanofibers embedded chitosan/tannin hydrogel with high antibacterial activity and hemostatic ability for drug-resistant bacterial infected wound healing, Carbohyd Poly. 12 (2023) 121687, https://doi.org/10.1016/j.carbpol.2023.121687.

[2] Y. Wu, Y. Wang, C. Zheng, C. Hu, L. Yang, Q. Kong, H. Zhang, Y. Wang, A versatile glycopeptide hydrogel promotes chronic refractory wound healing through bacterial elimination, sustained oxygenation, immunoregulation, and neovascularization, Adv. Funct. Mater. 33 (2023) 2305992, https://doi.org/10.1002/adfm.202305992.

[3] R. Zhang, B. Yu, Y. Tian, L. Pang, T. Xu, H. Cong, Y. Shen, Diversified antibacterial modification and latest applications of polysaccharide-based hydrogels for wound healthcare, Appl Mater Today, 26 (2022) 101396, https://doi.org/10.1016/j.apmt.2022.101396.

[4] R. Wilkening, C. Langouët-Astrié, M. Severn, M. Federle, A. Horswill, Identifying genetic determinants of Streptococcus pyogenes-host interactions in a murine intact skin infection model, Cell Rep. 42 (2023) 113332, https://doi.org/10.1016/j.celrep.2023.113332.

[5] Y. Hu, X. Ruan. X. Lv, Y. Xu, W. Wang, Y. Cai, M. Ding, H. Dong, J. Shao, D. Yang, X. Dong, Biofilm microenvironment-responsive nanoparticles for the treatment of bacterial infection, Nano Today. 46 (2022) 101602, https://doi.org/10.1016/j.nantod.2022.101602.

[6] X. Lv, L. Wang, A. Mei, Y. Xu, X. Ruan, W. Wang, J. Shao, D. Yang, X. Dong, Recent nanotechnologies to overcome the bacterial biofilm matrix barriers, Small. 19 (2023) 2206220, https://doi.org/10.1002/smll.202206220.

[7] M. Malone, G. Schultz, Challenges in the diagnosis and management of wound infection, Br J Dermatol. 187 (2022) 159-166, https://doi.org/10.1111/bjd.21612.

[8] P. Prateeksha, V. Sharma, N. Nagpoore, V. Jadaun, C. Rao, B. Singh, Bacteria-responsive multidrug delivery nanosystem for combating long-term biofilm-associated infections, Adv. Funct. Mater. 33 (2023) 2214852, https://doi.org/10.1002/adfm.202214852.

[9] Y. Zhan, X. Hu, Y. Li, Y. Wang, H. Chen, C. A. Omolo, T. Govender, H. Li, F. Huang, L. Shi, X. Hu, Y. Liu, Antimicrobial hybrid amphiphile via dynamic covalent bonds enables bacterial biofilm dispersal and bacteria eradication, Adv. Funct. Mater. 33 (2023) 2214299, https://doi.org/10.1002/adfm.202214299.

[10] S. Brouwer, T. Rivera-Hernandez, B. Curren, N. Harbison-Price, D. Oliveira, M. Jespersen, M. Davies, M. Walker, Pathogenesis, epidemiology and control of group a streptococcus infection, Nat Rev Microbiol. 21 (2023) 431-447, https://doi.org/10.1038/s41579-023-00865-7.

[11] G. Syrogiannopoulos, J. Nelson, Duration of antimicrobial therapy for acute suppurative osteoarticular infections, The Lancet, 331(1988) 37 – 40, https://doi.org/10.1016/S0140-6736(88)91013-6.

[12] S. Kaplan, Recent lessons for the management of bone and joint infections, J INFECTION. 68 (2013) S51-S56, https://doi.org/10.1016/j.jinf.2013.09.014.

[13] R. Zhang, Y. Tian, L. Pang, T. Xu, B. Yu, H. Cong, Y. Shen, Wound microenvironment-responsive protein hydrogel drug-loaded system with accelerating healing and antibacterial property, ACS Appl. Mater. Interfaces. 14 (2022) 10187-10199, https://doi.org/10.1021/acsami.2c00373.

[14] X. Ya, G. Li, P. Zhang, E. Jin, C. Xiao, X. Chen, Injectable Self-Healing Hydrogel Wound Dressing with Cysteine-Specific On-Demand Dissolution Property Based on Tandem Dynamic Covalent Bonds, Adv. Funct. Mater. 31 (2021) 2011230, https://doi.org/10.1002/adfm.202011230.

[15] N. Gong, A.G. Hamilton & M.J. Mitchell, A hydrogel-entrapped live virus immunization. Nat. Biomed. Eng. 7 (2023) 849–850, https://doi.org/10.1038/s41551-023-01008-2.

[16] L. Zhou, Y. Xi, Y. Xue, M. Wang, Y. Liu, Y. Guo, B. Lei, Injectable Self-Healing Antibacterial Bioactive Polypeptide-Based Hybrid Nanosystems for Efficiently Treating Multidrug Resistant Infection, Skin-Tumor Therapy, and Enhancing Wound Healing. Adv. Funct. Mater. 29 (2019) 1806883, https://doi.org/10.1002/adfm.201806883.

[17] Y. Fang, T. Nie, G. Li, L. Wang, J. Du, J. Wu, Multifunctional antibiotic hydrogel doped with antioxidative lycopene-based liposome for accelerative diabetic wound healing, Chem. Eng. J. 480 (2024) 147930, https://doi.org/10.1016/j.cej.2023.147930.

[18] O. Ciofu, C. Moser, P.Ø. Jensen, Tolerance and resistance of microbial biofilms. Nat. Rev. Microbiol. 20 (2024) 621–635, https://doi.org/10.1038/s41579-022-00682-4.

[19] A. Peschel, HG. Sahl, The co-evolution of host cationic antimicrobial peptides and microbial resistance. Nat. Rev. Microbiol. 4 (2006) 529–536, https://doi.org/10.1038/nrmicro1441.

[20] K. Brogden, Antimicrobial peptides: pore formers or metabolic inhibitors in bacteria?. Nat. Rev. Microbiol. 3 (2005) 238–250, https://doi.org/10.1038/nrmicro1098.

[21] Y. Tian, L. Pang, R. Zhang, T. Xu, S. Wang, B. Yu, L. Gao, H. Cong, Y. Shen, Poly-tetrahydropyrimidine antibacterial hydrogel with injectability and self-healing ability for curing the purulent subcutaneous infection, ACS Appl. Mater. Interfaces. 12 (2020) 50236-50247, https://doi.org/10.1021/acsami.0c13822.

[22] X. Li, S. Guo, S. Zhang, C. Li, B. Yu, H. Cong, Y. Shen, Preparation of antibacterial antiviral nanofiber and its application in durable and self-cleaning personal protective equipment, Chem. Eng.

J. 479 (2024) 147770, https://doi.org/10.1016/j.cej.2023.147770.
[23] X. He, P. Shi, T. Wu, B. Yu, H. Cong, Y. Shen, Preparation and application of high-efficiency, antibacterial, and antiviral PET–PTHP fibers, ACS Appl. Mater. Interfaces. 15 (2023) 48660–48672, https://doi.org/10.1021/acsami.3c10788.
[24] W. Li, H. Chen, J. Cai, M. Wang, X. Zhou, L. Ren, Poly(pentahydropyrimidine)-based hybrid hydrogel with synergistic antibacterial and pro-angiogenic ability for the therapy of diabetic foot ulcers, Adv. Funct. Mater. 33 (2023) 2303147, https://doi.org/10.1002/adfm.202303147.
[25] S. Guo, B. Yu, A. Ahmed, H. Cong, Y. Shen, Synthesis of polyacrylonitrile/polytetrahydropyrimidine (PAN/PTHP) nanofibers with enhanced antibacterial and anti-viral activities for personal protective equipment, J. Hazard. Mater. 424 (2022) 127602, https://doi.org/10.1016/j.jhazmat.2021.127602.
[26] C. Nunes-Alves, Targeting (p)ppGpp disrupts biofilms, Nat. Rev. Microbiol. 12 (2014) 461, https://doi.org/10.1038/nrmicro3302.
[27] H. Koo, R. Allan, R. Howlin, P. Stoodley, L. Hall-Stoodley, Targeting microbial biofilms: current and prospective therapeutic strategies, Nat. Rev. Microbiol. 15 (2017) 740–755, https://doi.org/10.1038/nrmicro.2017.99.
[28] T. Zhang, W. An, J. Sun, F. Duan, Z. Shao, F. Zhang, T. Jiang, X. Deng, C. Boyer, W. Gao, N-Terminal lysozyme conjugation to a cationic polymer enhances antimicrobial activity and overcomes antimicrobial resistance, Nano Lett. 22 (2022) 8294–8303, https://doi.org/10.1021/acs.nanolett.2c03160.
[29] S. Yan, S. Chen, X. Gou, J. Yang, J. An, X. Jin, Y.-W. Yang, L. Chen, H. Gao, Biodegradable supramolecular materials based on cationic polyaspartamides and pillar[5] arene for targeting gram-positive bacteria and mitigating antimicrobial resistance, Adv. Funct. Mater. 29 (2019) 1904683, https://doi.org/10.1002/adfm.201904683.
[30] J. Poole, C. J. Day, M. Itzstein, J. C. Paton, M. P. Jennings, Glycointeractions in bacterial pathogenesis. Nat. Rev. Microbiol. 16 (2018) 440–452, https://doi.org/10.1038/s41579-018-0007-2.
[31] S. Tao, Y. Li, J. Zhou, J. Qian, R. Schnaar, Y. Zhang, I. J. Goldstein, H. Zhu, J. P. Schneck, Lectin microarrays identify cell-specific and functionally significant cell surface glycan markers, Glycobiology, 18 (2008) 761-769, https://doi.org/10.1093/glycob/cwn063.
[32] J. Hyun, C. Lee, H. Lee, W. Jang, I. Shin, Bacterial Lectin-Targeting Glycoconjugates for Selective Elimination of Pathogenic Bacteria, ACS Macro Lett. 10 (2020) 1429-1432, https://doi.org/10.1021/acsmacrolett.0c00454.
[33] Y. Tian, R. Zhang, B. Guan, Y. Zhu, L. Chen, Oxydextran-based photodynamic antibacterial nanoplatform with broad-Spectrum antibacterial activity, Int J Bio Macromol. 236 (2023) 123917, https://doi.org/10.1016/j.ijbiomac.2023.123917.
[34] B. Wei, W. Li, Z. Zhao, A. Qin, R. Hu, B. Tang, Metal-free multicomponent tandem polymerizations of alkynes, amines, and formaldehyde toward structure- and sequence-controlled luminescent polyheterocycles, J. Am. Chem. Soc. 139 (2017) 5075-5084, https://doi.org/10.1021/jacs.6b12767.
[35] X. Zhang, K. Ren, C. Xiao, X. Chen, Guanosine-driven hyaluronic acid-based supramolecular hydrogels with peroxidase-like activity for chronic diabetic wound treatment, Acta Biomater. 172 (2023) 206-217, https://doi.org/10.1016/j.actbio.2023.10.014.
[36] P. Wan, W. Guo, Y. Wang, M. Deng, C. Xiao, X. Chen, Photosensitizer-polypeptide conjugate for effective

elimination of candida albicans biofilm, Adv Healthc Mater. 11 (2022) 2200268, https://doi.org/10.1002/adhm.202200268.

[37] J. Liu, Z. Zhang, Y. Yan, X. Zhang, C. Xiao, X. Chen, Microrod crystals formed via Rhein-mediated mineralization, Chem Commun. 59 (2023) 10169, https://doi.org/10.1039/d3cc02527f.